

# Investigation of the impact of water absorption on retinal OCT imaging in the 1060 nm range

**Marschall, Sebastian; Pedersen, Christian; Andersen, Peter E.**

*Published in:*
Biomedical Optics Express

*Link to article, DOI:*
10.1364/BOE.3.001620

*Publication date:*
2012

*Document Version*
Publisher's PDF, also known as Version of record

Biomedical Optics EXPRESS

# Investigation of the impact of water absorption on retinal OCT imaging in the 1060 nm range

**Sebastian Marschall, Christian Pedersen, Peter E. Andersen***

*DTU Fotonik, Department of Photonics Engineering, Technical University of Denmark, Frederiksborgvej 399, 4000 Roskilde, Denmark*

**peta@fotonik.dtu.dk*

**Abstract:** Recently, the wavelength range around 1060 nm has become attractive for retinal imaging with optical coherence tomography (OCT), promising deep penetration into the retina and the choroid. The adjacent water absorption bands limit the useful bandwidth of broadband light sources, but until now, the actual limitation has not been quantified in detail. We have numerically investigated the impact of water absorption on the axial resolution and signal amplitude for a wide range of light source bandwidths and center wavelengths. Furthermore, we have calculated the sensitivity penalty for maintaining the optimal resolution by spectral shaping. As our results show, with currently available semiconductor-based light sources with up to 100–120 nm bandwidth centered close to 1060 nm, the resolution degradation caused by the water absorption spectrum is smaller than 10%, and it can be compensated by spectral shaping with negligible sensitivity penalty. With increasing bandwidth, the resolution degradation and signal attenuation become stronger, and the optimal operating point shifts towards shorter wavelengths. These relationships are important to take into account for the development of new broadband light sources for OCT.



**OCIS codes:** (170.4500) Optical coherence tomography; (170.4460) Ophthalmic optics and devices; (350.5730) Resolution.

## References and links

1. D. Huang, E. A. Swanson, C. P. Lin, J. S. Schuman, W. G. Stinson, W. Chang, M. R. Hee, T. Flotte, K. Gregory, C. A. Puliafito, and J. G. Fujimoto, "Optical coherence tomography," Science **254**, 1178–1181 (1991).
2. S. Marschall, B. Sander, M. Mogensen, T. M. Jørgensen, and P. E. Andersen, "Optical coherence tomography—current technology and applications in clinical and biomedical research," Anal. Bioanal. Chem. **400**, 2699–2720 (2011).
3. B. L. Danielson and C. Y. Boisrobert, "Absolute optical ranging using low coherence interferometry," Appl. Opt. **30**, 2975–2979 (1991).
4. T. Hillman and D. Sampson, "The effect of water dispersion and absorption on axial resolution in ultrahigh-resolution optical coherence tomography," Opt. Express **13**, 1860–1874 (2005).
5. S. Hariri, A. A. Moayed, A. Dracopoulos, C. Hyun, S. Boyd, and K. Bizheva, "Limiting factors to the OCT axial resolution for in-vivo imaging of human and rodent retina in the 1060nm wavelength range," Opt. Express **17**, 24304–24316 (2009).
6. T. J. van den Berg and H. Spekreijse, "Near infrared light absorption in the human eye media," Vis. Res. **37**, 249–253 (1997).
7. Y. Coello, B. Xu, T. L. Miller, V. V. Lozovoy, and M. Dantus, "Group-velocity dispersion measurements of water, seawater, and ocular components using multiphoton intrapulse interference phase scan," Appl. Opt. **46**, 8394–8401 (2007).

#165201 - $15.00 USD Received 27 Mar 2012; revised 31 May 2012; accepted 8 Jun 2012; published 18 Jun 2012

8. W. Drexler and J. G. Fujimoto, "State-of-the-art retinal optical coherence tomography," Prog. Retin. Eye Res. **27**, 45–88 (2008).
9. W. Drexler, U. Morgner, F. X. Kärtner, C. Pitris, S. A. Boppart, X. D. Li, E. P. Ippen, and J. G. Fujimoto, "In vivo ultrahigh-resolution optical coherence tomography," Opt. Lett. **24**, 1221–1223 (1999).
10. B. Potsaid, I. Gorczynska, V. J. Srinivasan, Y. Chen, J. Jiang, A. Cable, and J. G. Fujimoto, "Ultrahigh speed spectral / Fourier domain OCT ophthalmic imaging at 70,000 to 312,500 axial scans per second," Opt. Express **16**, 15149–15169 (2008).
11. B. Považay, K. Bizheva, B. Hermann, A. Unterhuber, H. Sattmann, A. F. Fercher, W. Drexler, C. Schubert, P. K. Ahnelt, M. Mei, R. Holzwarth, W. J. Wadsworth, J. C. Knight, and P. S. J. Russel, "Enhanced visualization of choroidal vessels using ultrahigh resolution ophthalmic OCT at 1050 nm," Opt. Express **11**, 1980–1986 (2003).
12. A. Unterhuber, B. Považay, B. Hermann, H. Sattmann, A. Chavez-Pirson, and W. Drexler, "In vivo retinal optical coherence tomography at 1040 nm - enhanced penetration into the choroid," Opt. Express **13**, 3252–3258 (2005).
13. Y. Yasuno, Y. Hong, S. Makita, M. Yamanari, M. Akiba, M. Miura, and T. Yatagai, "In vivo high-contrast imaging of deep posterior eye by 1-$\mu$m swept source optical coherence tomography and scattering optical coherence angiography," Opt. Express **15**, 6121–6139 (2007).
14. M. L. Wolbarsht, A. W. Walsh, and G. George, "Melanin, a unique biological absorber," Appl. Opt. **20**, 2184–2186 (1981).
15. A. W. Sainter, T. A. King, and M. R. Dickinson, "Effect of target biological tissue and choice of light source on penetration depth and resolution in optical coherence tomography," J. Biomed. Opt. **9**, 193–199 (2004).
16. Y. Chen, D. L. Burnes, M. de Bruin, M. Mujat, and J. F. de Boer, "Three-dimensional pointwise comparison of human retinal optical property at 845 and 1060 nm using optical frequency domain imaging," J. Biomed. Opt. **14**, 024016 (2009).
17. B. Považay, B. Hermann, A. Unterhuber, B. Hofer, H. Sattmann, F. Zeiler, J. E. Morgan, C. Falkner-Radler, C. Glittenberg, S. Blinder, and W. Drexler, "Three-dimensional optical coherence tomography at 1050 nm versus 800 nm in retinal pathologies: enhanced performance and choroidal penetration in cataract patients," J. Biomed. Opt. **12**, 041211 (2007).
18. Y. Wang, J. S. Nelson, Z. Chen, B. J. Reiser, R. S. Chuck, and R. S. Windeler, "Optimal wavelength for ultrahigh-resolution optical coherence tomography," Opt. Express **11**, 1411–1417 (2003).
19. B. Potsaid, B. Baumann, D. Huang, S. Barry, A. E. Cable, J. S. Schuman, J. S. Duker, and J. G. Fujimoto, "Ultrahigh speed 1050nm swept source / Fourier domain OCT retinal and anterior segment imaging at 100,000 to 400,000 axial scans per second," Opt. Express **18**, 20029–20048 (2010).
20. C. Chong, T. Suzuki, K. Totsuka, A. Morosawa, and T. Sakai, "Large coherence length swept source for axial length measurement of the eye," Appl. Opt. **48**, D144–50 (2009).
21. D. C. Adler, W. Wieser, F. Trepanier, J. M. Schmitt, and R. A. Huber, "Extended coherence length Fourier domain mode locked lasers at 1310 nm," Opt. Express **19**, 20930–20939 (2011).
22. W. Wieser, B. R. Biedermann, T. Klein, C. M. Eigenwillig, and R. Huber, "Multi-megahertz OCT: High quality 3D imaging at 20 million A-scans and 4.5 Gvoxels per second," Opt. Express **18**, 14685–14704 (2010).
23. T. Klein, W. Wieser, C. M. Eigenwillig, B. R. Biedermann, and R. Huber, "Megahertz OCT for ultrawide-field retinal imaging with a 1050 nm Fourier domain mode-locked laser," Opt. Express **19**, 3044–3062 (2011).
24. S.-H. Yun, G. J. Tearney, J. F. de Boer, and B. E. Bouma, "Motion artifacts in optical coherence tomography with frequency-domain ranging," Opt. Express **12**, 2977–2998 (2004).
25. R. Huber, D. C. Adler, V. J. Srinivasan, and J. G. Fujimoto, "Fourier domain mode locking at 1050 nm for ultra-high-speed optical coherence tomography of the human retina at 236,000 axial scans per second," Opt. Lett. **32**, 2049–2051 (2007).
26. M. Kuznetsov, W. Atia, B. Johnson, and D. Flanders, "Compact ultrafast reflective Fabry-Perot tunable lasers for oct imaging applications," Proc. SPIE **7554**, 75541F (2010).
27. S. Marschall, T. Klein, W. Wieser, B. R. Biedermann, K. Hsu, K. P. Hansen, B. Sumpf, K.-H. Hasler, G. Erbert, O. B. Jensen, C. Pedersen, R. Huber, and P. E. Andersen, "Fourier domain mode-locked swept source at 1050 nm based on a tapered amplifier," Opt. Express **18**, 15820–15831 (2010).
28. S. Marschall, T. Klein, W. Wieser, T. Torzicky, M. Pircher, B. R. Biedermann, C. Pedersen, C. K. Hitzenberger, R. Huber, and P. E. Andersen, "Broadband Fourier domain mode-locked laser for optical coherence tomography at 1060 nm," Proc. SPIE **8213**, 82130R (2012).
29. M. K. Harduar, A. Mariampillai, B. Vuong, X. Gu, B. A. Standish, and V. X. D. Yang, "Dual-core ytterbium fiber amplifier for high-power 1060 nm swept source multichannel optical coherence tomography imaging," Opt. Lett. **36**, 2976–2978 (2011).
30. K. F. Palmer and D. Williams, "Optical properties of water in the near infrared," J. Opt. Soc. Am. **64**, 1107–1110 (1974).
31. American National Standards Institute, "American National Standard for Safe Use of Lasers," ANSI Z 136-1.
32. International Electrotechnical Commission, "Safety of laser products," IEC 60825.
33. B. R. Biedermann, W. Wieser, C. M. Eigenwillig, G. Palte, D. C. Adler, V. J. Srinivasan, J. G. Fujimoto, and R. Huber, "Real time en face Fourier-domain optical coherence tomography with direct hardware frequency demodulation," Opt. Lett. **33**, 2556–2558 (2008).

#165201 - $15.00 USD Received 27 Mar 2012; revised 31 May 2012; accepted 8 Jun 2012; published 18 Jun 2012

34. M. P. Minneman, J. Ensher, M. Crawford, and D. Derickson, "All-semiconductor high-speed akinetic swept-source for OCT," Proc. SPIE **8311**, 831116 (2011).
35. P. Schiebener, J. Straub, J. M. H. L. Sengers, and J. S. Gallagher, "Refractive index of water and steam as function of wavelength, temperature and density," J. Phys. Chem. Ref. Data **19**, 677–717 (1990).
36. M. Wojtkowski, V. Srinivasan, T. Ko, J. Fujimoto, A. Kowalczyk, and J. Duker, "Ultrahigh-resolution, high-speed, Fourier domain optical coherence tomography and methods for dispersion compensation," Opt. Express **12**, 2404–2422 (2004).

## 1. Introduction

During the past two decades, optical coherence tomography (OCT) [1] has become a well-established imaging technique for biomedical research and clinical diagnostics [2]. OCT is being applied in numerous fields, such as cardiology, dermatology, developmental biology, and first and foremost in ophthalmology. Due to the unique ability to generate non-invasively cross-sectional in vivo images of the human retina, OCT has become an important tool for early diagnosis of retinal diseases and for monitoring medical treatment.

One of the prominent advantages of OCT is the high axial resolution in the micrometer or even submicrometer range. The resolution depends primarily on the spectral bandwidth of the used light source. For a Gaussian spectrum with full width at half maximum (FWHM) $\Delta\nu_{3\,\mathrm{dB}}$ in optical frequency, the axial resolution, $\delta z$, in a medium with refractive index $n$ is

$$\delta z = \frac{2\ln 2}{\pi}\frac{c}{n\,\Delta\nu_{3\,\mathrm{dB}}} \tag{1}$$

$$\approx \frac{2\ln 2}{\pi}\frac{\lambda_c^2}{n\,\Delta\lambda_{3\,\mathrm{dB}}} \approx 0.44\frac{\lambda_c^2}{n\,\Delta\lambda_{3\,\mathrm{dB}}}, \tag{2}$$

where $c$ is the speed of light and $\Delta\lambda_{3\,\mathrm{dB}}$ is the corresponding bandwidth on the wavelength scale at the center wavelength $\lambda_c$.

However, the axial resolution is also influenced by chromatic dispersion and by spectrally dependent attenuation of any media that the probing light has to pass [3–5]. In case of retinal imaging, the performance is to a large extent governed by the properties of water, the main constituent of the ocular media [6, 7]. A double pass through the anterior eye segment and the vitreous body adds up to a path length of about 50 mm exhibiting wavelength-dependent dispersion and absorption.

Most OCT systems for retinal imaging operate at a center wavelength in the 800 nm range [8], primarily due to negligible absorption by water. Furthermore, well-developed broadband light sources are available, e. g. titanium:sapphire short-pulse lasers, which offer ultra-high axial resolution [9]. Silicon detector arrays with large pixel numbers enable the implementation of fast spectrometer-based frequency-domain OCT (FD-OCT) systems [10].

During the past few years however, the wavelength range around 1060 nm, where water absorption has a local minimum (Fig. 1), found increasing interest for imaging the retina and the underlying choroid [11–13], which provides the photoreceptor cells with oxygen and nutrients. In this range, attenuation by melanin is lower [14], hence more light is transmitted through the retinal pigment epithelium. Reduced scattering at higher wavelengths generally enables deeper penetration into the tissue [15, 16], and it is beneficial for imaging in eyes affected by a cataract [17]. Furthermore, chromatic dispersion in water is low around 1000 nm, which helps maintaining a high axial resolution [18].

For wavelengths above 1000 nm, the preferred OCT method utilizes wavelength-swept laser light sources, so-called *swept sources*, rather than a broadband light source and a spectrometer, because available detector arrays based on indium gallium arsenide have relatively low pixel numbers, which leads to a limited imaging depth range [19]. Swept-source OCT can provide

#165201 - $15.00 USD Received 27 Mar 2012; revised 31 May 2012; accepted 8 Jun 2012; published 18 Jun 2012

long ranging depths [19–21] and ultra-high image acquisition speed [22, 23], and it is more robust against motion artifacts [24]. Continuing research focuses therefore on the development of high-performance swept sources for the 1060 nm range [20, 23, 25–28].

A variety of broadband light sources for OCT in the 1060 nm band enable high axial resolution, e. g. superluminescent diodes (SLDs) or swept sources with spectra wider than 110 nm [5, 26, 29], or supercontinuum light sources spanning more than 200 nm [11]. However, the range of low water absorption is a relatively narrow window. For propagation through 50 mm water, the FWHM of the local minimum is roughly 100 nm (Fig. 1), which limits the applicability of ultra-broadband light sources. The parts of a light source spectrum that extend into the surrounding absorption bands are subject to increased attenuation, which narrows the transmitted spectrum and reduces the effective axial resolution of the OCT system. Although this is an important issue for light source development, no detailed analysis of the effect of water absorption in retinal imaging has been published until now.

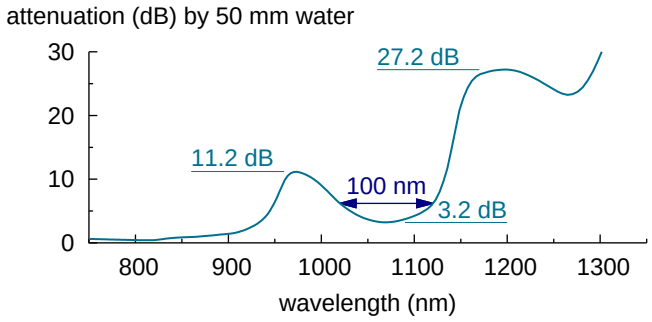


Fig. 1. In addition to the wavelength range below 950 nm, there is a minimum of the water absorption around 1060 nm, that permits in vivo OCT imaging of the human retina. For a length of 50 mm water—corresponding to a double pass through a human eye—this window has a 3 dB-width of approximately 100 nm. Calculated from data by Palmer and Williams [30].

A possible way to compensate for the water absorption is *spectral shaping*, i. e. adapting the light source spectrum such that it has the desired shape after propagation through water [4, 5]. Since one has to distribute a larger fraction of the optical power into the absorption bands, this method leads to higher average attenuation. The total incident power on the eye is limited by the maximum permissible exposure defined by the laser safety standards [31, 32]; hence, maintaining the axial resolution brings a penalty in signal strength or sensitivity, respectively, which increases with the light source bandwidth. This raises the question: how broad a bandwidth is actually useful for OCT in the 1060 nm band? Or more specifically: what is the trade-off between resolution and sensitivity depending on the light source bandwidth?

As Hariri et al. concluded earlier, 2 µm resolution in tissue could be achieved with a hypothetical light source generating a Gaussian spectrum truncated at ∼1120 nm after water absorption [5]. They did, however, not quantify the large fraction of the probing light that would be lost in the 975 nm-absorption band. Experimentally, the authors compared the resolution achievable with a regular SLD and a modified SLD featuring an increased spectral peak at 970 nm. In the case of a double pass through 25 mm water, the modified SLD yielded a minor improvement of the axial resolution. However, as this light source did not permit arbitrary spectral shaping, the question about the feasibility of true absorption compensation remained unanswered.

A detailed analysis of the topic has again become highly relevant due to recent develop-

#165201 - $15.00 USD Received 27 Mar 2012; revised 31 May 2012; accepted 8 Jun 2012; published 18 Jun 2012

ments in swept source technology. With new semiconductor laser gain media, broadband swept sources spanning the 1060 nm window have become available. Since the gain in semiconductors can be regulated rapidly by modulation of the pump current, arbitrary spectral shaping becomes straight-forward with these swept sources [23, 28, 33, 34]. However, as the implementation of OCT systems and light sources, especially swept sources, becomes more and more challenging with increasing bandwidth, it is important to know a priori whether a broad spectrum can be used effectively.

By numerical simulation, we have investigated the impact of water absorption on retinal imaging, covering a wide range of bandwidths and center wavelengths in the 1060 nm range. We computed axial point spread functions (PSFs), as they would be generated in a simple interferometer, and determined the peak broadening and the reduction of amplitude when including water absorption (Fig. 2(a)). Furthermore, we calculated the additional amplitude drop resulting from compensation of the broadening by spectral shaping.

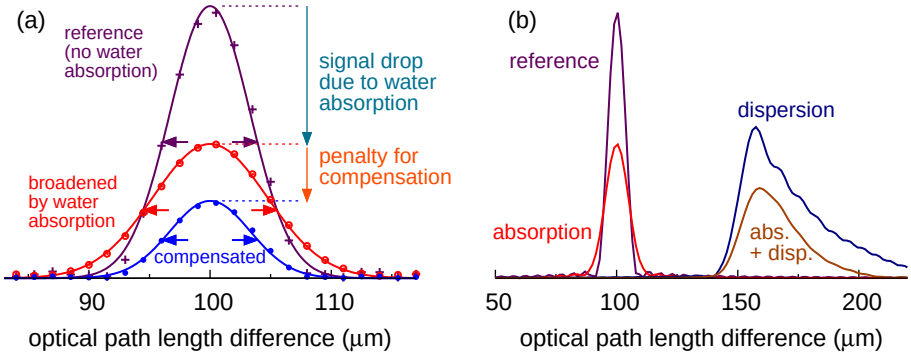


Fig. 2. Point spread functions (PSFs) calculated using a $1/e^2$-truncated Gaussian spectrum centered at 280 THz (∼1071 nm) with 60 THz total width (∼232 nm). (a) Key figures of the numerical investigation: PSF broadening and amplitude drop due to the water absorption compared to reference PSF, and additional amplitude drop due to compensation of the broadening by spectral shaping. Data points: calculated values; curves: fitted Gaussian. (b) Comparison of the broadening effects of absorption and dispersion. Refractive index data by Schiebener et al. [35].

For selected cases, we calculated PSFs including dispersion in order to compare its effect with that of absorption. In fact, with a wide light source spectrum, dispersion can often cause a significantly stronger broadening and distortion of the PSF peak than absorption does (Fig. 2(b)). However, since numerical compensation for dispersion is possible [4, 36], we have performed our analysis looking exclusively at the effects of absorption. For a detailed investigation of the influence of different dispersion orders, we may refer the reader to the work of Hillman and Sampson [4].

As our results show, the axial resolution achievable with current state-of-the art swept sources or SLDs with a bandwidth up to 120 nm is not severely affected by water absorption, provided the spectrum is centered close to 1060 nm. The resolution degradation is less than 10%, and it can be compensated by spectral shaping with minimal loss of sensitivity. The impact increases drastically when the bandwidth exceeds 150 nm. As the bandwidth increases, the optimal operating point with lowest sensitivity drop shifts to lower center wavelengths. This is an important relationship to be taken into account for the development of new broadband light sources.

#165201 - $15.00 USD Received 27 Mar 2012; revised 31 May 2012; accepted 8 Jun 2012; published 18 Jun 2012

## 2. Method

We implemented a script in Mathematica, that simulates the interference of two beams from the same light source in a simple interferometer, and computes the corresponding point spread function (PSF) from the resulting signal. As reference, we take an interferogram assuming light propagating through free-space in both interferometer arms, and calculate another one including the absorption profile of 50 mm water in one arm. In addition to overall attenuation of the amplitude, absorption changes the spectral shape of the interferogram envelope. Stronger attenuation towards the edges of the spectrum effectively narrows the spectral envelope, which leads to a broadening of the PSF peak. By comparing the PSFs in the cases with and without water absorption, we determine the loss of resolution and signal amplitude. Furthermore, we calculate a light source spectrum compensating for the water absorption profile. We normalize it to the same average power as the initial spectrum, but distribute a larger fraction of power into the absorption bands to restore the original interferogram shape. The resulting additional reduction of the PSF amplitude is a measure of the sensitivity penalty for maintaining the axial resolution.

The effect of dispersion, if included, is a non-linear distortion of the interferogram phase. This "chirp" can be compensated by multiplying the interferogram in its complex analytical representation with a wavelength-dependent phase term that cancels out the non-linearity. In practice, this phase term can for example be found by iteratively optimizing the image contrast [36].

Important for us, the influence of chromatic dispersion in water can be treated independently of absorption, and it can be compensated numerically. Hardware compensation, i. e. placing an equivalent length of water into the reference path of an OCT system, is not recommendable, since this would also aggravate the narrowing of the interferogram envelope by the water absorption. We can thus ignore chromatic dispersion in our analysis, and focus exclusively on the effect of absorption. Obviously, also the interferogram envelope can be manipulated numerically. In a real system, however, numerical spectral shaping is not an adequate method to compensate for absorption effects, since it would degrade the signal-to-noise ratio.

In our analysis, we consider light source spectra with a finite width,

$$I_0(\nu)\begin{cases} >0 & \text{if } |\nu-\nu_c| \le \frac{1}{2}\Delta\nu \\ =0 & \text{if } |\nu-\nu_c| > \frac{1}{2}\Delta\nu \end{cases}, \tag{3}$$

where $\nu_c$ is the central optical frequency and $\Delta\nu$ is the full width of the spectrum.

In order to determine the sensitivity penalty, we compare the signal amplitudes achieved with different spectra normalized to equal average intensity. In case of a swept source, we may have to take a non-linear sweep into account. For an given spectral envelope, $I(\nu)$, we calculate the time-averaged intensity $\langle I\rangle$ by integrating over one sweep period, $\tau_{sw}$, of the time-dependent light source frequency, $\nu_l(t)$:

$$\langle I\rangle = \frac{1}{\tau_{sw}}\int_0^{\tau_{sw}} I(\nu_l(t))dt. \tag{4}$$

With the average intensity thus calculated, we normalize the light source spectrum:

$$I_{0n}(\nu) = \frac{I_0(\nu)}{\langle I_0\rangle}. \tag{5}$$

After transmission through a length, $l$, of water, the spectrum changes according to the Beer-Lambert law:

$$\begin{aligned} I_{0a}(\nu) &= I_{0n}(\nu)\,T(\nu) \\ &= I_{0n}(\nu)\,\exp[-\mu_a(\nu)l]. \end{aligned} \tag{6}$$

#165201 - $15.00 USD Received 27 Mar 2012; revised 31 May 2012; accepted 8 Jun 2012; published 18 Jun 2012

For the absorption coefficient, $\mu_a$, we use an interpolation of the values reported by Palmer and Williams [30].

Assuming perfect elimination of the auto-correlation terms, e. g. by balanced detection, and neglecting chromatic dispersion in water, the detector signal generated with an interferometer path length difference $d$ is

$$V_{0n}(\nu) = \alpha I_{0n}(\nu) \cos\left(\tfrac{2\pi}{c}\nu d\right), \qquad \text{(without absorption)} \tag{7}$$

$$\begin{aligned} V_{0a}(\nu) &= \alpha \sqrt{I_{0n}(\nu) I_{0a}(\nu)} \cos\left(\tfrac{2\pi}{c}\nu d\right) \\ &= \alpha \sqrt{T(\nu)} I_{0n}(\nu) \cos\left(\tfrac{2\pi}{c}\nu d\right), \qquad \text{(with absorption in one arm)} \end{aligned} \tag{8}$$

where $\alpha$ is a constant conversion factor describing the detector response. For our analysis, we are comparing the amplitudes of different signals, not calculating absolute values. Hence, we assume $\alpha = 1$ in all calculations.

In order to yield an interferogram with the original spectral envelope after water absorption, we calculate a compensating spectrum and normalize it:

$$I_c(\nu) = \frac{I_0(\nu)}{\sqrt{T(\nu)}}, \tag{9}$$

$$I_{cn}(\nu) = \frac{I_c(\nu)}{\langle I_c \rangle}. \tag{10}$$

The resulting detector signal assuming water absorption in one interferometer arm,

$$V_{ca}(\nu) = \alpha \sqrt{T(\nu)} I_{cn}(\nu) \cos\left(\tfrac{2\pi}{c}\nu d\right) \tag{11}$$

$$= \alpha \frac{I_0(\nu)}{\langle I_c \rangle} \cos\left(\tfrac{2\pi}{c}\nu d\right) \tag{12}$$

$$= V_{0n}(\nu) \frac{\langle I_0 \rangle}{\langle I_c \rangle}, \tag{13}$$

has the same shape as $V_{0n}$, but a lower amplitude.

To quantify the effect of water absorption with and without spectral compensation, we calculate $V_{0n}$, $V_{0a}$, and $V_{ca}$, using $l = 50$ mm and $d = 0.5$ mm. From these interferograms, we compute the corresponding PSF with a discrete Fourier transform (DFT). For the DFT, we sample all interferograms from 200 THz to 400 THz in 0.1 THz steps, which produces a sufficient number of equally spaced data points in all PSFs. Finally, we determine the amplitude, $a$, and 3 dB-width, $w$, of the PSF peaks by fitting a Gaussian function to the data points. Comparison of $a$ in the three cases yields the signal drop caused by the water absorption, and $w/2$ is the corresponding axial resolution in air.

For our investigation, there are two quantities of interest: the relative broadening of the PSF peak due to the water absorption, $w_{0a}/w_{0n}$, and the drop of the signal amplitude with and without compensation relative to the reference, $a_{0a}/a_{0n}$ and $a_{ca}/a_{0n}$. The signal drop is plotted here on a $20 \times \log_{10}$ scale, which corresponds to the decrease in OCT sensitivity in decibels.

To determine the feasibility of broad bandwidth we use a Gaussian spectrum truncated at the $1/e^2$-points:

$$I_{0,Gauss}(\nu) = \begin{cases} \exp\left[-8\left(\frac{\nu-\nu_c}{\Delta\nu}\right)^2\right] & \text{if } |\nu-\nu_c| \le \frac{1}{2}\Delta\nu \\ 0 & \text{if } |\nu-\nu_c| > \frac{1}{2}\Delta\nu \end{cases} \tag{14}$$

This spectral shape (Fig. 3) results in an adequate compromise between a narrow PSF peak and low side lobes (Fig. 2), and it is simple to realize with a semiconductor-based swept

#165201 - $15.00 USD Received 27 Mar 2012; revised 31 May 2012; accepted 8 Jun 2012; published 18 Jun 2012

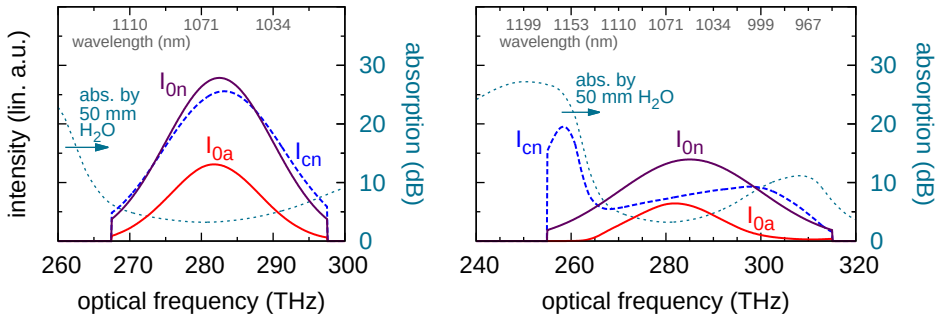


Fig. 3. The shape of a state-of-the-art broadband spectrum (left, $\Delta\nu = 30$ THz) changes only slightly due to water absorption, and compensation would require only a minor redistribution of power from the center to the edges. An ultra-broadband spectrum (right, $\Delta\nu = 60$ THz) gets strongly attenuated below 265 THz, and a large fraction of the total power is required to compensate for this. $I_{0n}$ and $I_{cn}$ are normalized to unity power.

source. For comparison, $\Delta\nu$ and the FWHM, $\Delta\nu_{3\mathrm{dB}}$, of the Gaussian function are related by $\Delta\nu = \sqrt{2/\ln 2}\,\Delta\nu_{3\mathrm{dB}} \approx 1.7\,\Delta\nu_{3\mathrm{dB}}$.

For normalizing the average power, we assume the most non-linear sweep characteristics found in typical swept sources: sinusoidal tuning of the wavelength. This is for instance the case with a resonantly tuned Fabry-Perot filter, and it results in a frequency sweep

$$\nu_l(t) = \left\{ \tfrac{1}{\nu_{max}} + \tfrac{1}{2}\left(\tfrac{1}{\nu_{min}} - \tfrac{1}{\nu_{max}}\right)\left[1+\sin\left(2\pi\,\tfrac{t}{\tau_{sw}}\right)\right]\right\}^{-1}, \tag{15}$$

where $\nu_{max} = \nu_c + \Delta\nu/2$ and $\nu_{min} = \nu_c - \Delta\nu/2$.

Under these conditions, we calculate the PSF broadening and the signal drop for $\nu_c$ ranging from 275 THz to 290 THz and $\Delta\nu$ ranging from 5 THz to 60 THz. This parameter space covers the center frequencies in the low-absorption range and the bandwidth relevant for OCT. 60 THz is about twice the bandwidth achievable with state-of-the-art swept sources or single SLDs, and it is roughly as wide as the broadest light source spectrum demonstrated for the 1060 nm window [11]. With $\Delta\nu = 60$ THz, a large fraction of the spectrum overlaps with the water absorption bands (Fig. 3, right), hence broader bandwidths are hardly feasible for OCT in this spectral range.

In addition, we examine the influence of a number of other system parameters, such as the spectral shape, the sweep characteristics, or water in both interferometer arms. As two extreme cases, we use a rectangular spectrum, $I_{0,Rect}(\nu)$, and a Hann-shaped spectrum,

$$I_{0,Hann}(\nu) = \begin{cases} 1+\cos\left(2\pi\,\frac{\nu-\nu_c}{\Delta\nu}\right) & \text{if } |\nu-\nu_c| \le \frac{1}{2}\Delta\nu \\ 0 & \text{if } |\nu-\nu_c| > \frac{1}{2}\Delta\nu \end{cases}, \tag{16}$$

which falls off smoothly to zero on both sides. This leads to a PSF with lower side-lobes and a peak that is about 20% broader than the PSF generated with $I_{0,Gauss}$. In contrast, $I_{0,Rect}$ yields a 25% narrowing of the PSF peak compared to $I_{0,Gauss}$, but increases the side-lobes drastically which in turn may limit the dynamic range in OCT.

Using $I_{0,Gauss}$, we determine the change in the sensitivity penalty for compensating the PSF broadening, when we assume a linear frequency sweep. Finally, we compare the influence of these parameters on the PSF broadening and the signal drop with the influence of water ab-

#165201 - $15.00 USD Received 27 Mar 2012; revised 31 May 2012; accepted 8 Jun 2012; published 18 Jun 2012

sorption in both interferometer arms. For the latter calculation, we replace the term $\sqrt{T(\nu)}$ in Eqs. 8, 9 and 11 with $T(\nu)$.

## 3. Results

With a bandwidth below 25 THz (90–100 nm), the resolution degrades by less than 10% at all center frequencies covered by the simulation (Fig. 4). The broadening increases fastest with the bandwidth at the low center frequencies, which are closest to the steep absorption band edge. Maintaining the resolution would bring here a considerable sensitivity penalty that increases rapidly for bandwidths above 25 THz (Fig. 5(a)). As expected, the lowest signal drop with a low or moderate bandwidth can be achieved with a sweep spectrum centered on the water absorption minimum (Fig. 5(b)), whereas a high center frequency leads to the slowest increase of the signal drop—with and without compensation—and would be of advantage for bandwidths broader than 40 THz (Fig. 5(c)).

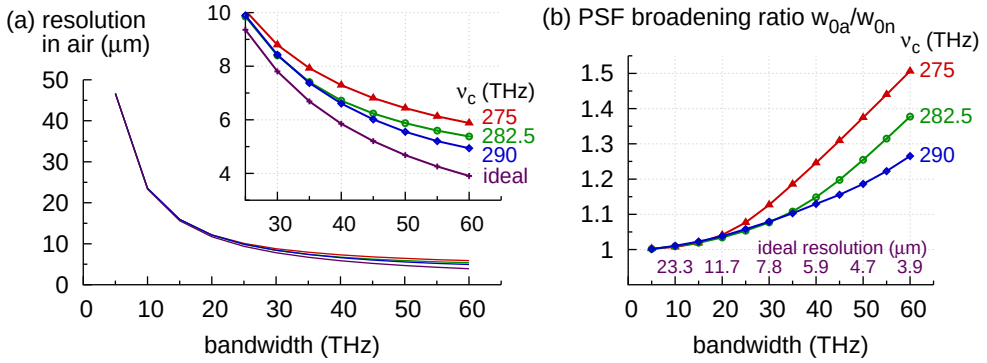


Fig. 4. (a) Calculated values for the axial resolution in air depending on the bandwidth at different center frequencies compared to the ideal reference case without water absorption. (b) The corresponding relative broadening ratios.

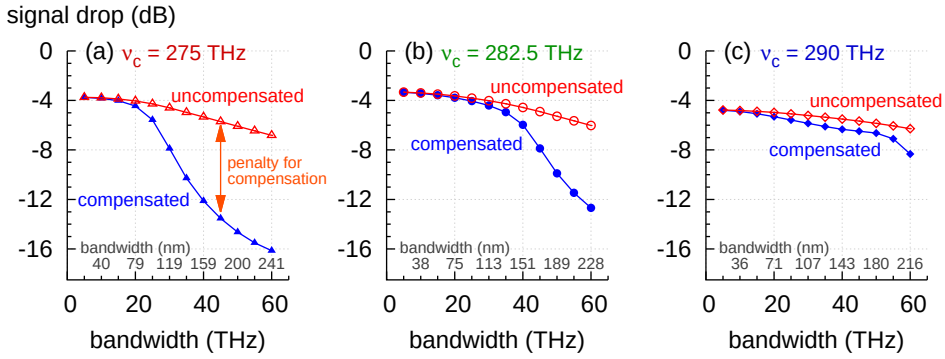


Fig. 5. Drop of the point spread function amplitude due to water absorption as a function of the bandwidth at different center frequencies with and without compensation for the broadening.

#165201 - $15.00 USD Received 27 Mar 2012; revised 31 May 2012; accepted 8 Jun 2012; published 18 Jun 2012

The PSF broadening and the signal drop as function of the center frequency reveal the same relationships (Fig. 6), but this visualization is more useful for choosing the optimal operating point for a given bandwidth. With a moderate bandwidth of 30 THz, the resolution degradation is almost constant in the range of the simulation (Fig. 6(a)). It only rises slightly if $\nu_c \leq 280$ THz. The signal drop (Fig. 6(b)) is lowest at $\nu_c = 280$–$282$ THz (1065–1070 nm) and the penalty for compensating the resolution degradation is negligible (Fig. 6(c)). If the bandwidth increases, the resolution degrades significantly faster at the low center frequencies, and the point of minimal signal drop shifts to higher frequencies. With the uncompensated spectrum, the signal drop varies only slightly, by less than 1 dB. However, the penalty for maintaining the resolution by absorption compensation becomes highly dependent on the center frequency, because of the steep absorption band edge on the long-wavelength side. The transmitted spectrum is virtually clipped at ∼1140 nm, and a large fraction of the incident power needs to be sacrificed for compensating these losses.

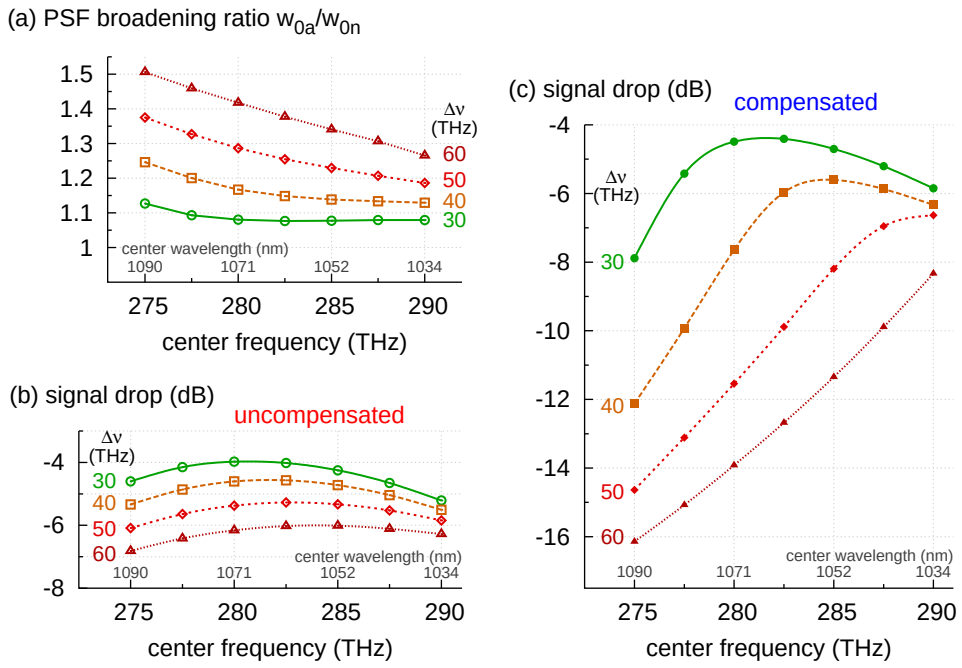


Fig. 6. (a) Relative broadening of the point spread function and (b, c) drop of the amplitude as a function of the center frequency for different bandwidths with and without compensation for the broadening.

A maximum PSF broadening ratio of 1.5 in the entire parameter space may seem unexpectedly low. However, the central part of the spectrum is in all cases within the low-absorption range. Therefore, the interferograms loose less than half of their total width. It is also important that we assume water absorption only in one interferometer arm. Inserting an equivalent amount of water into the reference path, e. g. for dispersion compensation, would lead to a more severe broadening of the PSF.

As comparing the effect of different operating parameters reveals, the influence of the spectral shape on the PSF broadening is relatively small (Fig. 7(a)). Both the Gaussian and the rectangular spectrum lead to about 40% broadening for $\nu_c = 282.5$ THz and $\Delta\nu = 60$ THz. With

#165201 - $15.00 USD Received 27 Mar 2012; revised 31 May 2012; accepted 8 Jun 2012; published 18 Jun 2012

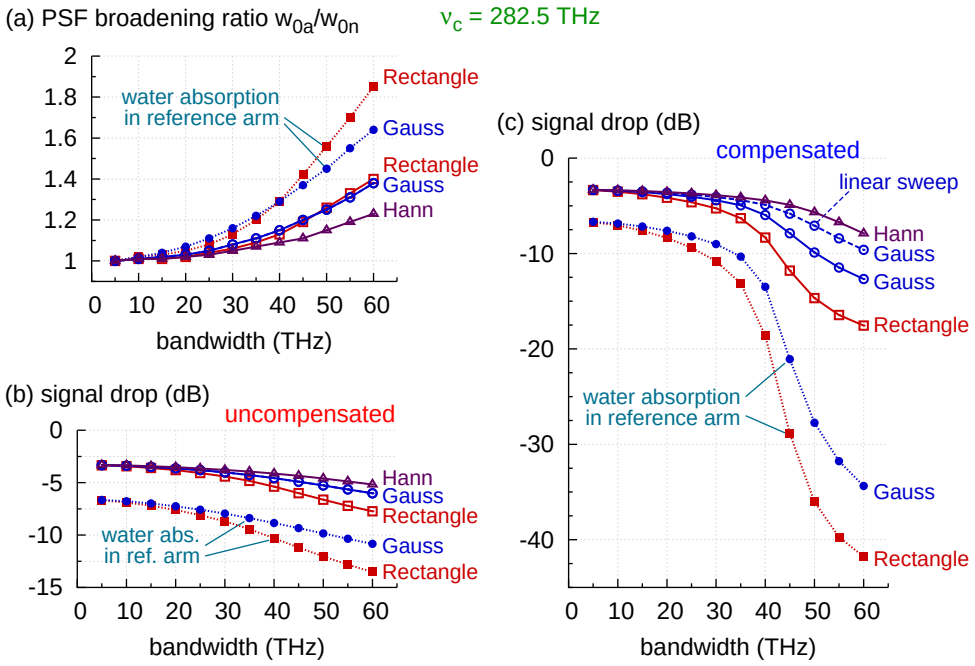


Fig. 7. (a) Relative broadening of the point spread function and (b, c) drop of the amplitude as a function of the bandwidth for different operating parameters with and without compensation for the broadening.

the Hann spectrum it is slightly lower, namely 23%. In contrast, the broadening ratio would increase drastically due to water absorption in the reference arm, especially with a rectangular spectrum it goes up to 85%. It would also severely aggravate the signal drop (Fig. 7(b,c)), especially when compensating the PSF broadening at high bandwidths. The influence of the spectral shape on the signal drop is smaller, but still significant. With compensation, there is a difference of up to 10 dB between the retangular and the Hann-shaped spectrum. In this case, also the sweep characteristics play a role. With the linear sweep, which concentrates more of the time-averaged power in the center of the spectrum, the sensitivity penalty is up to 3 dB lower than with the sinusoidal sweep. It does not influence the PSF broadening or the signal drop without compensation, because it changes neither the shape of the interferogram envelope nor the amplitude ratio between the reference signal and the attenuated signal.

## 4. Conclusion and outlook

As our simulation reveals, current state-of-the-art swept sources and SLDs with bandwidths up to 25–30 THz ($\leq$ 120 nm) suffer little degradation of the resolution, less than 10%, if the sweep range is centered close to the water absorption minimum (1060–1070 nm). Maintaining the optimal resolution by spectral shaping is in this range possible with a negligible sensitivity penalty below 1 dB. The resolution limiting effect becomes severe when the bandwidth exceeds 40 THz ($\sim$150 nm). Then, the optimal operating range shifts to shorter wavelengths, because all spectra are virtually truncated at $\sim$1140 nm by the steep absorption band edge.

Our numerical study on the feasibility of broad bandwidth focuses on one spectral shape, but it is representative for the general trends. With the bandwidth of state-of-the-art semiconductor-

#165201 - $15.00 USD Received 27 Mar 2012; revised 31 May 2012; accepted 8 Jun 2012; published 18 Jun 2012

based light sources, water absorption is not a severely limiting factor for the axial resolution, provided that the center wavelength is close to the absorption minimum. An extension of the bandwidth is feasible for improving the resolution, as long as the increasing sensitivity drop is acceptable within the particular system design. Especially if one aims for maintaining high resolution by spectral shaping, the center wavelength of the light source should match the range where the sensitivity drop is lowest. With increasing bandwidth, this optimal operating point shifts towards the short-wavelength side where the absorption band is significantly lower. This relationship is an important design criterion for the development of new broadband light sources.

Our simulation can also reveal how the resolution and the sensitivity drop depend on the spectrum and sweep characteristics of the light source. A linear frequency sweep is beneficial for compensating the resolution degradation at higher bandwidths. And as expected, spectral shapes with flat wings, such as the Hann function, are generally less affected by the water absorption, but yield lower axial resolution in the first place. Hence, our model can be used to choose the optimal combination of spectral shape, bandwidth, and center frequency for trading off resolution, sensitivity and dynamic range.

The model can easily be adapted and provides thus a framework for studying a variety of effects in OCT systems, for instance the influences of optical components in the imaging setup or chromatic dispersion in the beam path. Given the cost and technical challenges connected with extending the bandwidth of light sources and imaging systems, it becomes increasingly important to determine the optimal specifications early during the design process. Hence, this model is a valuable tool for future development of broadband light sources for OCT.

**Acknowledgments**

We would like to thank Robert Huber, Thomas Klein and Wolfgang Wieser at the Ludwig-Maximilians-Universität, München, for their helpful feedback on this work. We gratefully acknowledge the financial support from the European Union project FUN OCT (FP7 HEALTH, contract no. 201880).

#165201 - $15.00 USD Received 27 Mar 2012; revised 31 May 2012; accepted 8 Jun 2012; published 18 Jun 2012